The Geometry of Separation Boundaries: I. Basic Theory and Numerical Support

Angelo Lucia
Dept. of Chemical Engineering, University of Rhode Island, Kingston, RI 02881

Ross Taylor
Dept. of Chemical Engineering, Clarkson University, Potsdam, NY 13699

DOI 10.1002/aic.10668
Published online September 14, 2005 in Wiley InterScience (www.interscience.wiley.com).

Separation has always been an important task in the chemical industry. Even with the recent shift in emphasis and efforts to unify the physical and biological sciences, separation will remain an important workhorse in production and product/process design. The theory of simple distillation and residue curve maps has a long history—roughly 100 years—and has made a significant impact in the way many new separation processes are synthesized and designed. The key synthesis/design concept in this approach centers on understanding the ways in which constant boiling mixtures (or azeotropes) define separation boundaries. It is now well established that these azeotropes (or eutectics in melt or fractional crystallization and other solid–liquid separations) often define curved separation boundaries that place limitations on the degree of separation that can be achieved. Despite this, there remains no clear and exact understanding of separation boundaries and no straightforward way of accurately computing them in practice. A geometric methodology is presented that shows that exact separation boundaries can be defined through the use of differential geometry and dynamical systems theory and formulated as a constrained global optimization problem. Our novel approach is based on the observation that, for ternary homogeneous liquids, separation boundaries correspond to local maxima in the line integral within a given separation region. In addition, it is shown that these local maxima in the line integral correspond to one-sided cusps and that global optimization is absolutely necessary, given that several local maxima can exist within any separation region. Several numerical examples are presented that show that the proposed geometric approach can accurately find separation boundaries for homogeneous and heterogeneous mixtures. Finally, it is shown that our new methodology is very general and readily extends to mixtures with four or more components, reactive separations, nonequilibrium models, and other processes such as crystallization and vapor degreasing.
 AIChE J, 52: 582–594, 2006
Keywords: residue curves, separation boundaries, line integrals, global optimization, terrain methods

Introduction

Distillation and fractional crystallization have been the mainstays for separating chemical species and have been used extensively in a wide variety of industrial applications. Even with recent emphasis on product design, these unit operations will remain the workhorses of separation tasks in the chemical industry. Thus there will always be a need to understand the synthesis, design, or retrofitting of distillation and crystallization equipment to meet market demands. When the mixture to be separated contains azeotropic or eutectic points, limitations in the degree of separation by distillation and crystallization

Correspondence concerning this article should be addressed to A. Lucia at lucia@egr.uri.edu.

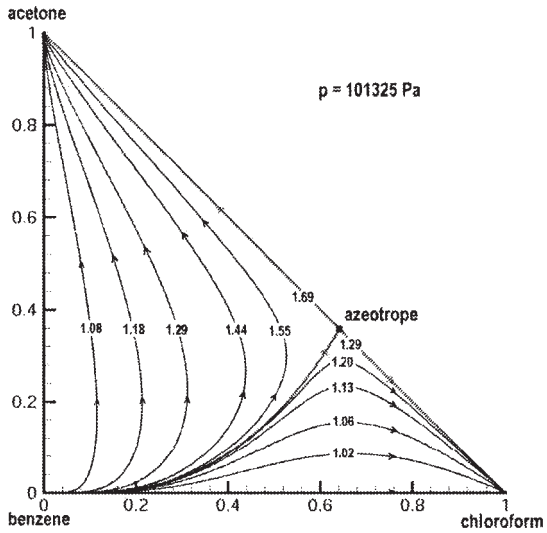

Figure 1. Residue curve map and line integrals for chloroform/acetone/benzene.

can exist. This is because azeotropes and eutectics can give rise to distinct separation regions and separation boundaries that cannot be crossed by open evaporation (that is, simple distillation) or open condensation. Thus, the presence of azeotropes and eutectics can directly affect the way a desired separation is designed and carried out.

During the early stages of the synthesis and design, residue curves are often used to provide insight into the behavior of separation by distillation and fractional crystallization. A *residue curve* is a trajectory that represents the solution to the set of ordinary differential mass balance and algebraic phase equilibrium equations that model a simple separator (such as simple distillation or simple crystallization; see, for example, Doherty and Perkins[1]). Moreover, although residue curves are often derived from the analysis of the separation behavior of open evaporation or open condensation, they also represent the behavior of either batch or continuous separations such as distillation and crystallization under limiting conditions (such as for a specific distillate removal policy in a batch rectification column or a continuous column at steady state and total reflux). Generally in the early stages of synthesis and design we are interested in knowledge that will help uncover feasible column designs for a range of feed conditions. Thus it is useful to construct a set of residue curves for different initial conditions. Usually these initial conditions are chosen so that the trajectories flow from the lowest to the highest boiling compounds. The corresponding collection of residue curves is called a *residue curve map*. One of the most important pieces of knowledge that comes from residue curve analysis is approximate knowledge of any separation boundaries that might exist.

To better understand the role that residue curve analysis plays in separation synthesis and design, consider the separation of a mixture of chloroform, acetone, and benzene at 101,325 Pa and the corresponding residue curve map shown in Figure 1. In this case, there is one maximum boiling binary azeotrope between chloroform and acetone that divides the composition space into two distinct distillation regions and a distillation boundary that runs from the benzene vertex to the chloroform–acetone azeotrope. Each residue curve within a specific distillation region can be viewed as the solution of the nonlinear differential equations given by

$$x' = y - x \tag{1}$$

where y denotes vapor composition in equilibrium with the liquid composition x. Given any set of initial conditions for the liquid composition, say $x(0)$, integration of Eq. 1 describes the behavior of the composition of the liquid remaining in a still pot under open evaporation (or, equivalently, liquid composition profile in an infinitely long continuous distillation column under total reflux). Now consider the task of designing a continuous distillation column to produce an acetone-rich overhead product. What any knowledgeable designer can tell immediately from the location and shape of the separation boundary in Figure 1 is that for any feed in the lower distillation region it is *not possible* to produce an overhead product rich in acetone by distillation alone. That is, regardless of the column design (such as number of stages or height of packing) or how it is operated (such as high or low reflux), the distillate product will always lie in the lower distillation region. This is because the distillation boundary cannot be crossed and thus places limitations on the composition of the overhead product. In fact, it is well known and widely accepted that trajectories cannot cross separation boundaries using open evaporation (or open condensation). Therefore, for any feed composition in the lower distillation region some other physical means of separation is required to cross the boundary and produce an acetone-rich product. This could be accomplished in a number of ways, such as by adding an entrainer to induce liquid–liquid behavior and then using decantation or using pressure-swing distillation to shift the location of the azeotrope. Moreover, it should be clear to the reader that all of this synthesis and design understanding comes from knowledge of the boundaries (that is, their location and shape) and that it applies to all types of separation processes: equilibrium or nonequilibrium stage or packed separations, batch separations, reactive separation processes, fractional crystallization, and others. Unfortunately, there are no precise ways of describing exact separation boundaries and no methodology for computing them in practice.

To make clear the key idea underlying this presentation, it is important to draw the reader's attention to the numbers associated with each residue curve in Figure 1. Each number represents the calculated distance along that trajectory (that is, the value of the line integral for that trajectory). Note that when all residue curves above and to the left of the distillation boundary are considered, the value of the line integral along the separation boundary is locally largest in this separation region. The same is true for the other separation region. This key observation—which seems to have been hiding in plain sight—is pivotal and provides the primary motivation for the novel geometric approach to separation boundaries presented herein. Moreover, as we will show later, the observation that separation boundaries for ternary homogeneous liquids correspond to line integrals of local maximum length generalizes to mixtures of four or more components, heterogeneous liquids, reactive separations, nonequilibrium processes, and other separations such as crystallization.

The remainder of this article is organized in the following

way. First, we provide a brief survey of the relevant literature followed by a description of the basic theory that underlies our new geometric approach to separation boundaries. Next various attributes of the optimization formulation required to compute separation boundaries are discussed. In particular, we give the steps of a feasible path optimization strategy for finding separation boundaries. This is followed by numerical results for a number of interesting ternary mixtures that demonstrate the efficacy of our geometric methodology and then general conclusions of this work. Finally, we show that the proposed approach generalizes to mixtures with four or more components, reactive separations, mass transfer–based models, crystallization, vapor degreasing, and other processes.

A Brief Literature Survey

The literature for residue curve maps (and distillation lines) is quite vast. We refer the reader to several extensive reviews on the subject (see, for example, Pöllmann and Blass,[2] Fien and Liu,[3] Widago and Seider,[4] and Kiva et al.[5]). In addition, the recent review of Kiva et al. is particularly noteworthy because it covers the relatively less well known but extensive and important contributions made by Russian researchers (see, also, Petlyuk[6]). Here we give only a brief survey of the results in this area that we feel are relevant to the material in the remainder of this presentation. Other relevant citations will be made throughout the text.

The first papers on residue curve maps date back to those of Ostwald[7,8] and Schreinemakers.[9-11] However, much of the current knowledge with respect to residue curves grows out of the work of Doherty and Perkins[1] and has been developed extensively by Doherty and coworkers for homogeneous mixtures,[12] heterogeneous mixtures,[13,14] and reactive mixtures[15-17] as it applies to the synthesis and design of distillation and reactive distillation. Slaughter and Doherty[18] extended the idea of residue curve maps to melt crystallization and call the associated collection of trajectories crystallization path maps (see, for example, Figures 9 and 10 in Slaughter and Doherty).

Despite the advances that have occurred in the development of residue curve maps, there is no precise definition and few definitive procedures for directly computing separation boundaries. In their text, Doherty and Malone[19] define distillation regions and distillation boundaries as follows:

> *Each distillation region must contain one unstable node, one stable node, and at least one saddle. Distillation regions are divided by distillation boundaries. There must be a saddle on at least one end of a distillation boundary.*

For many years, it was believed that simple distillation boundaries coincided with the ridges and valleys in boiling point surfaces. Although van Dongen and Doherty[20] convincingly demonstrated that simple boundaries do *not* coincide with the ridges and valleys of any boiling temperature surfaces, a precise definition of a boundary or its relationship (if any) to thermodynamics or physics has, to date, remained elusive. On the other hand, numerical procedures for computing very approximate separation boundaries have been developed. These include the methods of Foucher et al.,[21] Peterson and Partin,[22] and the geometric method of Rooks et al.[23] Pöpken and Gmehling[24] recently extended the work of Rooks et al. and presented an algorithm for computing distillation boundaries for quaternary mixtures based on singularity theory. All current numerical methods find approximate separation boundaries of Eq. 1 (or equivalently $x' = x - y$).

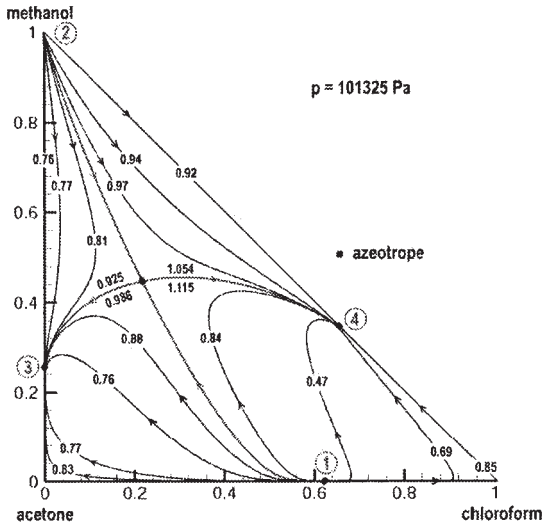

Figure 2. Residue curve map and line integrals for chloroform/methanol/acetone.

Maximum Line Integrals: A Geometric Characterization of Separation Boundaries

We begin our theoretical development by considering ternary homogeneous liquid mixtures. From differential geometry, any particular trajectory of Eq. 1 can be represented as a parameterized curve $x(\alpha)$ for $\alpha \in [0, T]$, where $x(0)$ and $x(T)$ are the end points of the trajectory. The key observation in defining separation boundaries for ternary homogeneous liquids is, as stated earlier, that the line integral (or distance along a trajectory) from an unstable node to a reachable stable node is a local extremum along a boundary. This is clearly illustrated in Figure 1, where the maximum distance of 1.69 along the separation boundary is greater than the length of any other trajectory in the region above and to the left that ends at the acetone vertex. The same is true for trajectories in the region below and to the right of that end at the chloroform vertex where the maximum distance of 1.29 along the boundary is greater than any other trajectory in that region. However, it is important to understand that it is the distance along the entire trajectory from unstable to stable node that must be measured for this key observation to be true. Also note that if the azeotrope in Figure 1 was somehow a minimum boiling azeotrope instead of a maximum boiling azeotrope, then the azeotropic composition would correspond to a stable node of Eq. 1, although that would change nothing about our key observation. In that case there would be one distillation region and the two trajectories of local maximum distance would correspond to the edges of the triangular diagram. The same is true for ideal or nonideal zeotropic mixtures.

Now consider a more complicated case in which there are several azeotropes and more than two distillation regions. In particular, consider the ternary mixture of chloroform, methanol, and acetone shown in Figure 2. In this case there are four azeotropes: three binary azeotropes and one ternary azeotrope. Two of the binary azeotropes are minimum boiling azeotropes

and are both stable nodes of Eq. 1; the other is maximum boiling and corresponds to an unstable node. The methanol vertex is also an unstable node with respect to Eq. 1. These nodes are denoted by the circled numbers in Figure 2 and thus nodes 1 and 2 are unstable, whereas nodes 3 and 4 are stable with respect to Eq. 1. The ternary azeotrope, on the other hand, is an intermediate boiling mixture and therefore a saddle point node of the differential equations in Eq. 1. Nonetheless, when any trajectory (or integral curve) from any unstable node to any reachable stable node is considered, the distance along the separation boundary is greater than any other neighboring trajectories in the same region, as shown in Figure 2. Note, however, in this example, there are some separation regions with more than one maximum in the line integral, clearly demonstrating that it is necessary to find all line integrals of maximum length in all separation regions to define separation boundaries with certainty.

This key observation leads to the following geometric characterization of separation boundaries in terms of line integrals. A separation boundary is the trajectory, say $x^*(\alpha)$, associated with the solution of the nonlinear programming problem

$$\max_{x(0)} D = \int_0^T \|x'(\alpha)\| d\alpha \tag{2}$$

subject to

$$x'(\alpha) = y[x(\alpha)] - x(\alpha) \tag{3}$$

$$x(T) = x_T \tag{4}$$

where D represents a line integral or distance function along a trajectory, $\|\cdot\|$ denotes the two-norm, $x(0)$ is any feasible set of initial conditions on the ball (or circle in the case of a ternary mixture) of radius ε about some designated unstable node x_0, and x_T is a stable node. We define the ball of radius ε about a designated unstable node x_0, by $B(x_0, \varepsilon) = \{x : \|x - x_0\| = \varepsilon$ for all $x\}$. Note that the objective function D in Eq. 2 is a function of only the initial conditions $x(0)$, which are the unknown variables, and any trajectory $x^*(\alpha)$ that corresponds to local optimal values of the unknown variables is a separation boundary. Also, it is implied that all azeotropic compositions (and temperatures) of a given mixture have been determined before solving Eqs. 2 to 4. Several good techniques are available for this purpose; however, we use the terrain methodology of Lucia and Yang[25] for finding all azeotropes because it is reliable and efficient.

Finding Separation Boundaries Using Optimization

To determine separation boundaries, we must solve the problem defined by Eqs. 2 to 4 for all constrained global maxima and there is flexibility for doing this in both the formulation as well as in the choice of optimization algorithm. That is, the problem defined by Eqs. 2 to 4 can be formulated as a feasible path optimization in which direct numerical integration is used and for which there are only $c - 1$ degrees of freedom (that is, the initial conditions of Eq. 1). Equations 2 to 4 could, on the other hand, be formulated as an infeasible path optimization. Here a discrete trajectory represented by say N points would be assumed between the unstable and stable nodes and these points would be constrained to satisfy discrete versions of the differential constraints $x' = y - x$ as well as boundary conditions. The infeasible path formulation has much larger storage requirements than the feasible path approach and it is not at all clear that it offers any real computational advantages in convergence, given that the constraints are generally highly nonlinear.

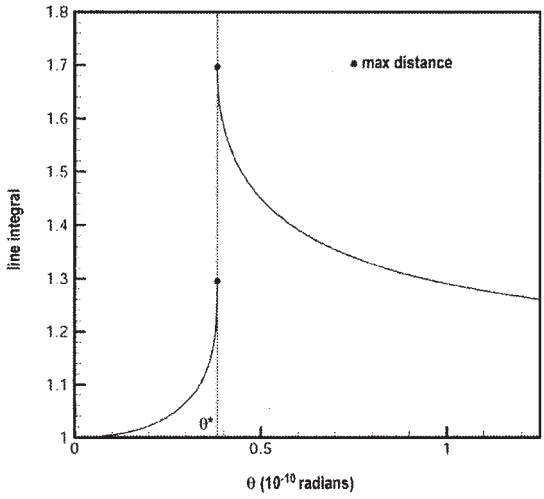

Figure 3. Line integral vs. theta for chloroform/acetone/benzene.

In our initial investigations, we have used a feasible path approach based on direct integration coupled with optimization to solve the problem defined by Eqs. 2 to 4. That is, given a set of feasible initial conditions, $x(0)$, defined on $B(x_0, \varepsilon)$, we integrate Eq. 1 (or equivalently Eq. 3) and determine the distance along a resulting trajectory. Because each trajectory is uniquely defined by initial conditions, this distance is a function of only the initial conditions. In spherical coordinates, this fact results in a single degree of freedom for any ternary mixture because $x(0)$ is related to both the radius (ε) and an angle of rotation (θ) through the simple relationship $x(0) = x_0 + \varepsilon[\cos\theta, \sin\theta]$. Thus D is a function of θ only for fixed ε. Therefore, by using optimization to adjust the initial conditions on $B(x_0, \varepsilon)$ in an intelligent way, we can maximize this distance. The resulting trajectory of maximum distance, $x^*(\alpha)$, is a separation boundary. Additional maxima can be found using global optimization and this will be described in detail in the Optimization Algorithm section. Note also that all of these concepts generalize to any number of components. For example, for four components a circle becomes a sphere, a line integral becomes a surface area integral, and one independent angle of rotation becomes two independent angles of rotation.

Many good techniques are available for solving the global optimization problem defined by Eqs. 2 to 4. These include deterministic methods such as tunneling,[26] the branch and bound approach (αBB) of Maranas and Floudas,[27] the interval methods of Stadtherr and coworkers,[28] and terrain methods.[25,29,30]. There are also stochastic global optimization methods such as simulated annealing,[31] genetic algorithms,[32] and methods based on stochastic differential equations[33] that can be

used. In this work we use terrain methodologies because they are reliable and efficient.

The Nature of Relevant Optima

For a ternary mixture and spherical coordinates, we are interested in finding all maxima of the function $D(\theta)$. Figure 3 clearly shows that, although $D(\theta)$ is smooth within any single separation region, it is discontinuous at an extremum and has the shape of a one-sided cusp. This is because $dD/d\theta$ approaches infinity and because the length of trajectories changes abruptly as any boundary is crossed in that either the unstable node, stable node, or both changes abruptly. Also note that as a separation boundary is crossed the slope of $dD/d\theta$ changes sign. In our opinion, it is important to understand and exploit these mathematical and physical facts associated with the shape and slope of $D(\theta)$ in designing numerical algorithms to find optima in this setting.

Feasible path optimization

The major computational tools needed to solve Eqs. 2 to 4 using a feasible path approach are an accurate numerical integrator and a robust global optimization methodology.

Numerical integrators

There are many numerical integration algorithms that can be used to solve the differential–algebraic equations that describe the dynamic behavior of Eq. 1. These include explicit methods such as forward Euler and Runge–Kutta integration; fully implicit methods such as the backward Euler and trapezoidal rule; multistep techniques such as Gear's method, which is based on backward-difference formulae (BDF); or semi-implicit integrators such as the family of semi-implicit Runge–Kutta methods. The most important thing here is that the integrator must be able to calculate accurate trajectories and line integrals. Our preliminary numerical experience shows that a method such as fourth-order Runge–Kutta is sufficient for this. Forward Euler, on the other hand, can give inaccurate results unless sufficiently small integration step sizes are used.

Numerical optimization

To apply terrain methods or any other Newton-based approach to the global optimization problem given by Eqs. 2 to 4, partial derivatives of distance with respect to initial conditions are required. These derivatives can be accumulated during the integration process from first and second partial derivatives of the right-hand side of Eq. 1 using techniques similar to the one described in Lucia et al.[34]

Partial derivatives

Partial derivatives of the line integral with respect to initial conditions can be calculated by recursion during the integration process. To see this, consider the integration of Eq. 1 from $x(\alpha)$ to $x(\alpha + \Delta\alpha)$ and the way in which D changes along the resulting trajectory. For convenience let $x(\alpha) = x_k$, $x(\alpha + \Delta\alpha) = x_{k+1}$, and $\Delta x_k = x_{k+1} - x_k$. The form of D in Eq. 2 implies that

$$\nabla_x[\|\Delta x_k\|] = [J_k^T - I]\Delta x_k/\|\Delta x_k\| \tag{5}$$

where J_k denotes the $(c-1)\times(c-1)$ matrix of partial derivatives of x_{k+1} with respect to x_k and, from the nonlinear differential equations defined by Eq. 1, is given by

$$J_k = I - h(J_{yx} - I) \tag{6}$$

The $(c-1)\times(c-1)$ matrix J_{yx} in Eq. 6 is the matrix of partial derivatives of y with respect to x and contains, of course, any implicit temperature derivatives with respect to x; h is an integration step size. The line integral in Eq. 2 can be approximated using the rule

$$D = \int_0^T \|x'(\alpha)\|d\alpha = \int_0^T (\|dx/d\alpha\|)d\alpha \approx \sum_{k=0}^{N} \|\Delta x_k\| \tag{7}$$

Straightforward differentiation of Eq. 7 from the initial conditions $x(0)$ to a stable node and the chain rule give

$$\begin{aligned}\nabla_{x(0)}D = \nabla_{x(0)}\left[\sum \|\Delta x_k\|\right] &= [J_0^T - I]\Delta x_0/\|\Delta x_0\| \\ &+ [J_1^T - J_0^T]J_0\Delta x_0/\|\Delta x_1\| + [J_2^T - J_1^T]J_1J_0\Delta x_0/\|\Delta x_2\| \\ &+ \cdots = \sum_0^N [J_k^T - J_{k-1}^T]\left[\prod_0^{k-1} J_j\right]\Delta x_0/\|\Delta x_k\|\end{aligned} \tag{8}$$

where the symbol Π denotes the product and where $J_{-1} = I$. Note that Eq. 8 clearly shows that the gradient of distance with respect to initial conditions can be computed during the integration process, provided the Jacobian matrix of the righthand side of the differential equation, J_{yx}, is available. The gradient of D with respect to $x(0)$ can, in turn, be related to the angle of rotation θ, through the simple expression

$$D' = dD/d\theta = -\varepsilon \sin\theta\,[\partial D/\partial x_1(0)] + \varepsilon\cos\theta\,[\partial D/\partial x_2(0)] \tag{9}$$

given that $x(0) = x_0 + \varepsilon[\cos\theta, \sin\theta]$. The subscripts 1 and 2 in Eq. 9 denote component indices. Calculation of the second derivative of D would require second partial derivatives of y with respect to x, which are tensor quantities. In our opinion, the second derivative D'' is most conveniently computed using the secant method (or a hybrid quasi-Newton method; see Venkataraman and Lucia[35]).

An Optimization Algorithm

In this section, we present a feasible path optimization algorithm for finding separation boundaries. The basic steps of the algorithm follow and are discussed in more detail where necessary below for the case of a ternary mixture with distillation as the separation process.

(1) Find all azeotropic points of the given mixture.
(2) Select an unstable node, x_0.

(3) Specify the radius $\varepsilon > 0$ and define the ball, $B(x_0, \varepsilon) = \{x : \| x - x_0 \| = \varepsilon\}$.

(4) Define $\theta_{\min}$ and $\theta_{\max}$.

(5) Set $j = 0$ and choose a feasible initial angle of rotation $\theta_{\min} \leq \theta_j \leq \theta_{\max}$.

(6) Calculate $x_j(0) = x_0 + \varepsilon[\cos\ \theta_j, \sin\ \theta_j]$.

(7) Generate the entire trajectory defined by $x' = y - x$ for $x_j(0)$.

During integration

(a) Accumulate $D(\theta_j) = \Sigma \| \Delta x_k \|$, where the summation is from $k = 0$ to N.

(b) Accumulate $D' = dD/d\theta_j$ using Eqs. 8 and 9.

(c) Calculate D''.

(d) Identify the stable node x_T, to which the integration converges.

(8) Check for an extremum in D. If D is optimal, stop; else go to step 9.

(9) Compute θ using $\theta_{j+1} = \theta_j - \beta D'/D''$ such that $\theta_{\min} \leq \theta_{j+1} \leq \theta_{\max}$, where β is a line search parameter.

(10) Calculate $x_{j+1}(0) = x_0 + \varepsilon[\cos\ \theta_{j+1}, \sin\ \theta_{j+1}]$, generate the entire trajectory defined by $x' = y - x$ for $x_{j+1}(0)$, and during integration

(a) Accumulate $D(\theta_{j+1}) = \Sigma \| \Delta x_k \|$, where the summation is from $k = 0$ to N.

(b) Accumulate $D' = dD/d\theta_{j+1}$ using Eqs. 8 and 9.

(c) Calculate D''.

(11) If x_T remains unchanged and $D(\theta_{j+1}) > D(\theta_j)$, set $j = j + 1$, and go to step 8; else reduce β and return to step 9.

Step 1 can be implemented in any number of ways; we use the terrain methods of Lucia and Yang[25] to find all of the azeotropes of the specified mixture. We must also determine which stationary points of Eq. 1 are unstable nodes, which are stable nodes, and which are saddles. For a ternary system this can often be done quite simply using the approach of Foucher et al.[21] (see also Doherty and Malone[19]). Alternatively, it is possible to determine the nature of each stationary point by computing the eigenvalues of the Jacobian of the right-hand side of Eq. 1. Step 2 requires us to select one of the unstable nodes. Step 3 defines the ball of radius ε that surrounds the unstable node. We suggest an initial value of $\varepsilon = 0.001$ for the radius, although for some systems it will be necessary to use a larger radius (example 3 in the Numerical Support section is a case in point). Step 4 defines the range of feasible rotation angles. For example, for an unstable node at the origin of a right triangle, the feasible angles fall in the range $0 \leq \theta \leq \pi/2$, and for an unstable node on the hypotenuse of a right triangle the feasible angles fall in the range $3\pi/4 \leq \theta \leq 7\pi/4$. In step 5 we select an initial feasible angle of rotation θ, whereas step 6 is the calculation of a point on the surface of the ball defined in step 3. This point serves as the initial conditions for the differential equations $x' = y - x$. Step 7 involves the (numerical) integration of these differential equations from the point near the unstable node to some stable node (determined not by us, but by the integration). As we perform the integration we simultaneously compute the line integral and its derivatives. This completes the preliminary calculations and, as a consequence, all quantities in steps 2 to 7 now will be defined in a consistent manner.

Steps 8 to 11 constitute the heart of the algorithm. Step 8 determines whether the current value of θ corresponds to an extremum in D; if so the algorithm terminates. The termination criterion we use is described in detail in the next paragraph of this section. Otherwise, a new estimate of the rotation angle is calculated in step 9 and a new trajectory, line integral, and its derivatives are evaluated in step 10. Step 11 ensures that the new trajectory ended at the same stable node as did the prior integration. We also ensure that there is an improvement (increase) in the line integral from iteration to iteration by using a line search procedure. This is important because the line integral is discontinuous at a local optimal solution. The line search function we use is based on the assumption that $D(\theta)$ is a (one-sided) cusp and for this we use the procedure outlined in Lucia and DiMaggio.[36] This cusp model, which is given by

$$D(\theta) = D_0 - [(\theta - \theta_c)^T A(\theta - \theta_c)]^{1/m} \tag{10}$$

where D_0 is a constant, θ_c is the location of the cusp, A is a positive scalar, and $m > 2$ is an integer, enables the use of a scaled Newton step in step 8, given that from Eq. 10 it follows that the unique optimum of the cusp is given by

$$(\theta - \theta_c) = [(2 - m)/m]D'(\theta)/D''(\theta) \tag{11}$$

Note that we do not need to know either D_0 or the scalar A in Eq. 10 to calculate a Newton correction to θ and that the scaled Newton step defined in Eq. 11 converges to the maximum in one iteration if $D(\theta)$ really is a cusp of order m. However, we do not know m or θ_c in advance. To circumvent this lack of knowledge, we let the line search parameter β, in the Newton step defined in step 9 of the algorithm, capture the effect of the term $[(2 - m)/m]$. Thus, Eq. 11 is replaced by the updating equation for θ given in step 9 of the algorithm. Once improvement is obtained, the algorithm returns to step 7 to begin a new iteration and this process (that is, steps 8 to 11) is repeated until convergence is reached. The trajectory $x^*(\alpha)$, which corresponds to the optimal value of θ^*, is one of possibly several separation boundaries.

Local optimality

Because $D(\theta)$ is one-sided differentiable, $D' = 0$ does not necessarily hold at a maximum point (see Figure 3). Thus there is some difficulty in determining when the algorithm has reached a local optimal solution and that is why we left the criterion in step 7 undefined. However, one convenient way of defining termination is to make use of knowledge of the pure component vertices and azeotropic compositions that correspond to saddle point nodes of Eq. 1. For a trajectory to be a boundary, it must pass through any relevant saddle point nodes (see Figure 1). Thus, in a numerical setting, termination can be defined by measuring how close a trajectory passes to a given set of relevant saddle point nodes. It is also possible to infer convergence from the fact that $dD/d\theta$ becomes extremely large at a separation boundary and changes sign as the boundary is crossed.

Finding all maxima from a single unstable node

To ensure that all local maxima from a given unstable node are located, we use the terrain methodology of Lucia et al.[30] to intelligently explore the range of feasible rotation angles, $\theta_{\min} \leq \theta \leq \theta_{\max}$. For example, from Figure 1, the range of feasible

rotation angles surrounding the unstable benzene vertex is $0 \leq \theta \leq \pi/2$. Once θ^* and the associated separation boundary $x^*(\alpha)$ are located using the proposed algorithm, the terrain methodology is used to explore this range of feasible rotation angles. The use of terrain methods has two consequences. First, if θ^* corresponds to an interior boundary, then the terrain methodology will locate all stable nodes from the given unstable node. Thus, in this case both the chloroform and acetone vertices will be located regardless of which is found first. This is because small perturbations of θ^* must result in the location of at least two stable nodes when $x^*(\alpha)$ is an interior separation boundary. Second, the terrain methodology is designed to follow the valleys and ridges of the surface $D(\theta)$ to locate other stationary points (that is, minima, saddle points, and maxima). Thus, other maxima for $\theta \in [\theta_{\min}, \theta_{\max}]$ will also be determined reliably and effectively, given that $D(\theta)$ is smooth within a given separation region. In Figure 2, for example, we observe four distinct trajectories of local maximum distance that run from the chloroform–acetone azeotrope (node 1) to either the chloroform–methanol azeotrope (node 4) or methanol–acetone azeotrope (node 3). Exactly two trajectories of local maximum distance correspond to interior separation boundaries and run through the ternary saddle point to either stable azeotropic node. The other two trajectories of local maximum distance are (1) the trajectory along the edges of the triangular region that runs from the chloroform–acetone azeotrope to the methanol–acetone azeotrope and (2) the trajectory that runs along the edges from the chloroform–acetone azeotrope to the chloroform–methanol azeotrope. All local maxima in line integral can be located using the terrain methodology. This example reinforces the need for using global optimization to solve the problem defined by Eqs. 2 to 4! We refer the reader to the studies reported by Lucia and coworkers[25,29,30] for more details of the terrain method.

Finding all local maxima from all unstable nodes

The proposed optimization algorithm must be applied from each unstable node of the multicomponent mixture under consideration. In the chloroform, methanol, acetone mixture shown in Figure 2, the algorithm must be applied twice—once from the chloroform–acetone azeotrope and once from the methanol vertex. Moreover, each unstable node has its own set of rotation angle constraints and there can be multiple local maxima associated with any given unstable node. This will be explained in more detail in the next section.

Numerical support

In this section, we give some numerical support for the approach outlined in the previous sections of this paper by providing numerical details for a number of example problems. All examples in this report use either the original UNIQUAC equation as described in Prausnitz et al.[37] or the NRTL equation of Renon and Prausnitz[38] to model the liquid phase. Binary interaction parameters for UNIQUAC and NRTL and Antoine or extended Antoine coefficients can be found in the Appendix. The vapor phase is assumed to be ideal. All azeotropic compositions and temperatures at the specified pressure were computed to an accuracy of $\| y - x \| < 10^{-10}$ using the terrain methodology of Lucia and Yang.[25] It is also instructive to note that we used a fourth-order Runge–Kutta method with a fixed integration step size of $h = 10^{-3}$ to generate trajectories of Eq. 1 for all examples herein. All computations were performed in double-precision arithmetic on a Pentium III computer equipped with a Lahey F77/90-EM32 compiler.

Example 1: Chloroform(1)/Acetone(2)/Benzene(3)

Figure 1 shows values of the line integral for various trajectories for the homogeneous liquid mixture chloroform/acetone/benzene at 101,325 Pa using the UNIQUAC equation to model the liquid phase. The purpose of this first example is to provide some of the details of the basic optimization ideas that underlie the calculation of the separation boundaries using the algorithm described in the previous section. For chloroform, acetone, and benzene at 101,325 Pa there is a single maximum boiling binary azeotrope between chloroform and acetone at a temperature of $T = 339.12$ K with a corresponding composition $x = (x_1, x_2, x_3) = (0.641399, 0.358601, 0)$. Benzene is the heavy component, with a boiling point of 354.28 K, and the benzene vertex is the only unstable node x_0 with respect to Eq. 1. Both the chloroform and acetone vertices are stable nodes of Eq. 1, whereas the binary chloroform–acetone azeotrope is a saddle node. All of this information can be (and is) determined before performing any integration or optimization calculations.

Let $\varepsilon = 10^{-3}$. For any ternary mixture with an unstable node at the origin, the feasible region is defined by $0 = \theta_{\min} \leq \theta \leq \theta_{\max} = \pi/2$ radians. Therefore, choose an initial feasible rotation angle of $\theta = \pi/4$ radians. As a result, the initial condition $x(0) = [x_1(0), x_2(0)] = (0.00707168, 0.00707168)$ is on the closed ball $B(x_0, \varepsilon)$ and lies in a region above and to the left in Figure 1. Moreover, the stable node of Eq. 1 to which this initial condition converges is the acetone vertex. From this starting point, the initial trajectory basically hugs the acetone–benzene axis and has a line integral value of $D = 1.00031338$. From here the proposed optimization algorithm converges to the optimal solution of $\theta^* = 3.829310180 \times 10^{-11}$ radians with an optimal value of the line integral of $D(\theta^*) = 1.6905316$. Moreover, it is easily verified by direct numerical simulation that the resulting boundary [or trajectory, $x^*(\alpha)$] in Figure 1 is longer than any other trajectory started from a feasible point in this region on $B(x_0, \varepsilon)$. On the other hand, for an initial rotation angle of $\theta = 0$ radians, the initial condition $x(0) = [x_1(0), x_2(0)] = (0.001, 0)$ is in the other separation region. In this case, our optimization algorithm converges to the same optimal angle and resulting boundary, only the corresponding optimal value of the line integral is $D(\theta^*) = 1.290593$. Once again, it is easy to verify that the resulting optimal trajectory $x^*(\alpha)$ is longer than any other trajectory started from a feasible point on $B(x_0, \varepsilon)$ in the region. Figure 3 shows the behavior of $D(\theta)$ in both distillation regions in the neighborhood of θ^*. Note that $D(\theta)$ is shaped like a one-sided cusp in each separation region, that it is discontinuous at each local maximum (that is, at the boundary), and that the stable vertex to which trajectories converge as well as the sign of $dD/d\theta$ both change as the boundary is crossed, all of which can be exploited in an algorithmic sense.

In reality we do not use multiple starting points. Rather, we use the terrain methodology to systematically explore, in this case, the feasible region defined by $\theta \in [0, \pi/2]$, once a first local maximum has been located. As a consequence, both

Table 1. Azeotropic Compositions and Temperatures for Chloroform(1)/Methanol(2)/Acetone(3) at 101,325 Pa

Composition	Temperature (K)
(0.653121, 0.346879, 0)	327.52
(0.641399, 0, 0.358601)	339.12
(0, 0.234284, 0.765716)	329.74
(0.217330, 0.447018, 0.335652)	331.71

stable vertices are easily located and the calculations also indicate that there are no additional local maxima in $D(\theta)$ because the terrain methodology encounters both bounds (that is, 0 and $\pi/2$) without any indication that there are other stationary points.

Example 2: Chloroform(1)/Methanol(2)/Acetone(3)

This liquid mixture, which is modeled by the UNIQUAC equation, is more complicated than Example 1. Moreover, the purpose of this second example is to illustrate the power of the proposed geometric approach to separation boundaries and the need for global optimization. Chloroform–methanol–acetone forms a homogeneous liquid mixture that has three binary azeotropes and a ternary azeotrope at 101,325 Pa, which were calculated using the terrain methodology of Lucia and Yang.[25] The resulting azeotropic compositions and temperatures are shown in Table 1. As can be seen from Table 1, two of the binary azeotropes are minimum boiling azeotropes (that is, chloroform–methanol and methanol–acetone); thus they are stable nodes of Eq. 1. The third binary azeotrope between chloroform and acetone is maximum boiling and together with the methanol vertex is an unstable node of Eq. 1. The saddle nodes of Eq. 1 are the ternary azeotrope, the chloroform vertex, and the acetone vertex.

Figure 2 shows line integral values for various trajectories in each of the four distillation regions for the mixture chloroform/methanol/acetone at 101,325 Pa. Note that each separation boundary is a local maximum in the value of the line integral. Table 2 shows that there are six values of θ that give six trajectories of maximum length and that four (really only two) of these values of θ^* correspond to boundaries within the triangular region. The other two values of θ^* correspond to trajectories along the edges of the triangular region.

The details of these computations are as follows. For the unstable chloroform–acetone azeotrope (node 1 in Figure 2), the feasible region is defined by $0 = \theta_{\min} \leq \theta \leq \theta_{\max} = \pi$ radians, $x_0 = (0.641399, 0)$, and $\varepsilon = 0.001$ as before. From an initial feasible value of $\theta_0 = \pi/2$, the terrain methodology actually converges to $\theta_2^* = 3.14159265313116$, which is very close to the value of π. The optimal value of the line integral $D(\theta_2^*)$ is 1.115032, as shown in Table 2, and it is easily verified that this is the largest distance of any trajectory in this region. Moreover, the resulting optimal trajectory $x_2^*(\alpha)$ corresponds to the interior separation boundary that runs from the chloroform–acetone azeotrope (node 1) through the ternary saddle point azeotrope to the chloroform–methanol azeotrope (node 4).

Terrain calculations from θ_2^* in the direction of smaller rotation angles move down and uphill on the surface $D(\theta)$ and show that there is a value of θ that is a minimum in the line integral as well as a second value of θ, say $\theta_1^* = 0$, that corresponds to a local maximum value of the line integral $D(\theta_1^*) = 0.849220$ in the region enclosed by the chloroform–acetone azeotrope, the chloroform vertex, and the chloroform–methanol azeotrope. It turns out that this second trajectory, say $x_1^*(\alpha)$, is the trajectory that runs along the edges of this portion of the triangular region. However, what's important is that the global optimization methodology finds this second local maximum (and the corresponding optimal distance and trajectory) without any prior knowledge. In addition, note that there is a part of the separation boundary, $x_2^*(\alpha)$, that is also part of the separation boundary that runs from the chloroform–acetone azeotrope (node 1) through the ternary saddle point azeotrope to the methanol–acetone azeotrope (node 3). Thus terrain calculations from θ_2^* in the direction of larger rotation angles easily find $\theta_3^* = 3.14159265313116$, $D(\theta_3^*) = 0.986485$, and the separation boundary $x_3^*(\alpha)$, which runs from the chloroform–acetone azeotrope through the ternary saddle to the methanol–acetone azeotrope. However, there is another trajectory of local maximum length in the region enclosed by node 1, the acetone vertex, and node 3. As before, this second trajectory of local maximum length is the trajectory along the edges of the triangle in this region corresponding to $\theta_4^* = \pi$, for which $D(\theta_4^*) = 0.873621$ and once again this path is also located by the terrain methodology—without any prior knowledge of this fact!

The proposed optimization algorithm must be applied a second time from the other unstable node: the methanol vertex (node 2 in Figure 2). For the unstable methanol vertex, the feasible region is defined by $3\pi/2 = \theta_{\min} \leq \theta \leq \theta_{\max} = 2\pi$ radians. Again we let $\varepsilon = 0.001$, set $x_0 = (0, 1)$, and choose an initial feasible rotation angle, $\theta_0 = 7\pi/8$. From here, the optimization algorithm easily converges to an optimal angle of $\theta_5^* = 4.77759842$ and the corresponding trajectory $x_5^*(\alpha)$, which defines the separation boundary from the methanol vertex to the chloroform–methanol azeotrope (node 4). Here the local maximum value of the line integral is $D(\theta_5^*) = 0.924528$. Subsequent terrain calculations initiated from θ_5^* easily find $\theta_6^* = 4.77759842$, $D(\theta_6^*) = 1.053566$, and the separation boundary $x_6^*(\alpha)$ from the methanol vertex to the methanol–acetone azeotrope and the fact that no other local maxima exist, again without any prior information regarding the number of maxima!

Table 2. Optimal Rotation Angles/Maximum Line Integrals for Chloroform(1)/Methanol(2)/Acetone(3) at 101,325 Pa

Rotation Angle (radians)	Maximum Line Integral
0	0.849220 (from node 1 to node 4)
3.14159265	1.115032 (from node 1 to node 4)
3.14159265	0.986485 (from node 1 to node 3)
π	0.873621 (from node 1 to node 3)
4.77759842	0.924528 (from node 2 to node 3)
4.77759842	1.053566 (from node 2 to node 4)

Table 3. Azeotropic Compositions and Temperatures for Methanol(1)/Acetone(2)/Methylacetate(3) at 101,325 Pa

Composition	Temperature (K)
(0.20585, 0.79415, 0)	328.48
(0.34539, 0, 0.65461)	327.03
(0, 0.59975, 0.40025)	328.05
(0.26999, 0.23523, 0.49478)	326.81

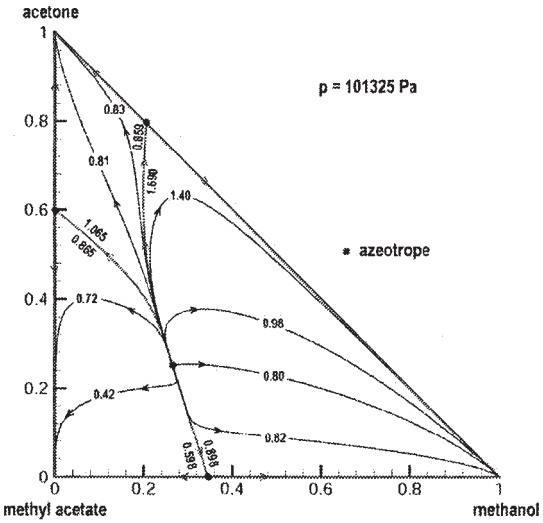

Figure 4. Residue curve map and line integrals for methanol/acetone/methylacetate.

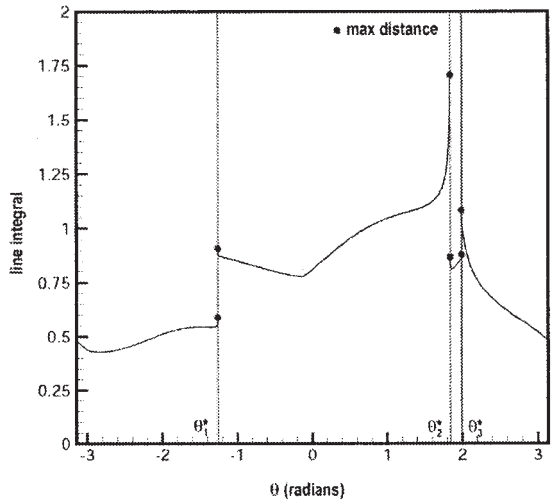

Figure 5. Line integral vs. theta for methanol/acetone/methylacetate.

Example 3: Methanol(1)/Acetone(2)/Methylacetate(3)

The third example is a mixture of methanol, acetone, and methylacetate at 101,325 Pa. The purpose of this example is to demonstrate the reliability of the proposed geometric approach in the case where portions of the separation boundaries are coincident over some part of the feasible region. This system forms a homogeneous liquid mixture and was modeled using the NRTL equation. The binary interaction parameters for the NRTL equation and coefficients for the Antoine equations for component vapor pressures were obtained from the well-known compilation of Gmehling and Onken[39] and are given in the Appendix. This mixture has three binary azeotropes as well as a minimum boiling ternary azeotrope, shown in Table 3. Unlike the previous example, the ternary azeotrope in this system is the lowest boiling mixture and thus the only stable node with respect to Eq. 1. The three binary azeotropes are saddle nodes, whereas the pure component vertices are unstable nodes of Eq. 1. The separation boundaries for this system run from the ternary azeotrope through each of the saddle points, ending at a pure component node.

Figure 4 shows line integral values for various trajectories for each of the three distillation regions for the methanol/acetone/methylacetate mixture at 101,325 Pa. Note, as before, each separation boundary is a local maximum in the line integral. However, it is important to note that a slightly different numerical approach was used to compute the residue curves and line integrals for this system to illustrate that there is flexibility in the way these computations can be implemented. In particular, for this example we actually integrated Eq. 1 backwards from the ternary azeotrope (that is, from low temperature to high temperature) because it is the only stable node of Eq. 1. This is perhaps more in line with most readers' experience in integrating residue curves, even though the direction of integration makes no difference. Clearly the distance is the same in either direction. However, we integrated Eq. 1 backwards because it allowed us to find all local maxima from a single node by simply considering the feasible region $-\pi = \theta_{\min} \leq \theta \leq \theta_{\max} = \pi$, which corresponds to a complete ε-circle around the stable node. Table 4 shows that there are six values of θ (really three) that give six trajectories of maximum length, all within the triangular region. All separation boundaries run from the ternary azeotrope to an appropriate binary saddle azeotrope and then each path branches in two directions along a corresponding binary axis to the respective pure component vertices.

Figure 5 shows the behavior of $D(\theta)$. Note that there are three separate discontinuities in $D(\theta)$, one for each separation boundary, as expected. However, two of the discontinuities are very close together. Moreover, it is important to note that Figure 4 was generated by adjusting the radius ε upward in the neighborhood of the separation boundaries near the ternary azeotrope. Values of 0.001 or even 0.01 did not allow us to find all optimal angles with sufficient precision to actually compute an accurate maximum in the line integral. This is because virtually all residue curves from the ternary saddle node are coincident along all portions of the separation boundaries for small values of ε, especially in the direction of the acetone vertex (see Figure 4). As a result, initial values on $B(x_0, \varepsilon)$ for

Table 4. Optimal Rotation Angles/Maximum Line Integrals for Methanol(1)/Acetone(2)/Methylacetate(3) at 101,325 Pa

Rotation Angle (radians)	Maximum Line Integral
−1.26102129435	0.898165 (from ternary azeo to methanol vertex)
−1.26102129445	0.588625 (from ternary azeo to methylacetate vertex)
1.83664633295	1.690305 (from ternary azeo to acetone vertex)
1.83664533295	0.858532 (from ternary azeo to methanol vertex)
1.98705084909	1.064692 (from ternary azeo to methylacetate vertex)
1.98705074909	0.865198 (from ternary azeo to acetone vertex)

Table 5. Azeotropic Compositions and Temperatures for Ethanol(1)/Benzene(2)/Water(3) at 101,325 Pa

Composition	Temperature (K)
(0.445058, 0.554942, 0)	341.07
(0.887440, 0, 0.112560)	352.19
(0, 0.606544, 0.393456)	335.10
(0.292561, 0.563017, 0.144422)	337.20

Table 6. Optimal Rotation Angle and Maximum Line Integrals for Ethanol(1)/Benzene(2)/Water(3) at 101,325 Pa

Rotation Angle (radians)	Maximum Line Integral
0	1.987153 (from water vertex to B/W azeotrope)
$3\pi/4$	1.240066 (from ethanol vertex to B/W azeotrope)
π	1.211855 (from ethanol vertex to B/W azeotrope)
$7\pi/4$	1.077071 (from benzene vertex to B/W azeotrope)

ε values of 0.001 or 0.01 are difficult to ascribe to a separation boundary, even in double-precision arithmetic. Thus many initial values converge to the pure component vertices before any of the binary saddle azeotropes are reached with these smaller values of ε. Remember we are integrating Eq. 1 backwards in this example. On the other hand, by increasing the radius (in this case to $\varepsilon = 0.21$) in the neighborhood of the boundaries it was relatively simple to find all optimum rotation angles corresponding to maximum line integrals. Note also that it is straightforward to recognize when trajectories that converge to different nodes are coincident on $B(x_0, \varepsilon)$ and to define a procedure to automatically increase the radius.

Example 4: Ethanol(1)/Benzene(2)/Water(3)

The final example is a liquid mixture of ethanol, benzene, and water at 101,325 Pa. Here, as in examples 1 and 2, the UNIQUAC equation was used to model the liquid phase and Eq. 1 is integrated in the forward direction (that is, from high- to low-temperature nodes). The purpose of this example is to illustrate that the proposed geometric methodology for finding separation boundaries can be applied directly to heterogeneous liquids. The ethanol/benzene/water mixture exhibits one ternary and three binary azeotropes. These azeotropic compositions and temperatures are shown in Table 5. Note that the benzene/water azeotrope is the only stable node with respect to Eq. 1. All other azeotropes are saddle nodes and the three pure component vertices are unstable nodes of Eq. 1.

Figure 6 shows the line integral values for a number of trajectories. Note that there are three distillation regions and actually two trajectories of local maximum length in the region

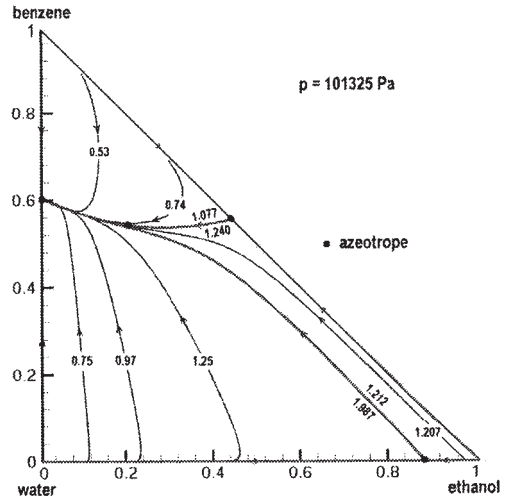

Figure 6. Residue curve map and line integrals for ethanol/benzene/water.

in the lower right-hand corner of Figure 6 (that is, near the ethanol vertex). The optimal rotation angles that correspond to maximum line integral values are shown in Table 6.

The details of the optimization calculations used to determine the separation boundaries in this example are as follows. For the water vertex, $x_0 = (0, 0)$ and the feasible region is defined by $0 = \theta_{\min} \leq \theta \leq \theta_{\max} = \pi/2$ radians. We set $\varepsilon = 0.001$ and chose an initial rotation angle of $\theta_0 = \pi/4$ radians. Accordingly, the terrain methodology converged easily to an optimal rotation angle of $\theta_1^* = 0$ radians. Actually the converged value of the rotation angle was a very small number (on the order of 10^{-20}) and the corresponding local maximum in the line integral is $D(\theta_1^*) = 1.987153$. This local optimal trajectory, $x_1^*(\alpha)$, hugs the ethanol–water axis until it reaches the ethanol–water azeotrope, then breaks sharply in a direction away from the ethanol–water axis, passes through the ternary saddle azeotrope, and finally converges to the benzene–water azeotrope, which is the stable node with respect to Eq. 1. Moreover, the calculations clearly show that the behavior of $D(\theta)$ is monotonically decreasing with decreasing rotation angle throughout the feasible region about the water vertex. On the other hand, for the ethanol vertex, $x_0 = (1, 0)$ and the feasible region is defined by $3\pi/4 = \theta_{\min} \leq \theta \leq \theta_{\max} = \pi$ radians. Using an initial rotation angle of $\theta_0 = 7\pi/8$ radians, the terrain method converged to $\theta_2^* = 3\pi/4$ radians and then $\theta_3^* = \pi$ radians after passing through a minimum in the line integral. The corresponding optimal values of the line integral are $D(\theta_2^*) = 1.240066$ and $D(\theta_3^*) = 1.211855$, respectively. Finally, behavior from the benzene vertex is very similar to that from the water vertex. There is a single maximum in the line integral of $D(\theta_4^*) = 1.077071$ that corresponds to an optimal rotation angle of $\theta_4^* = 7\pi/4$ radians.

Conclusions

A new geometric approach to defining exact separation boundaries was proposed. It was shown that separation boundaries correspond to local maxima in the line integral for ternary liquid mixtures and that these local maxima are one-sided cusps. It was also demonstrated that global optimization is necessary to find all separation boundaries with certainty because several local maxima in the line integral can exist within any given separation region. A feasible path optimization algorithm based on direct numerical integration, coupled with the terrain methodology of Lucia et al.,[30] was presented to compute separation boundaries. Numerical issues related to finding maxima in cusp functions and related convergence criteria were also described. Several numerical examples for homogeneous and heterogeneous ternary liquid mixtures were studied. Numerical results clearly show that our new geometric methodology for defining separation boundaries is easily imple-

mented on a computer and can correctly locate exact separation boundaries in a reliable manner.

Coda

We close this presentation with discussions of how the fundamental concept of line integrals for defining separation boundaries for ternary liquid mixtures can be extended to mixtures with four or more components, separations coupled with reactions, nonequilibrium (or mass transfer) models, other separations such as melt and fractional crystallization, and industrial cleaning processes such as vapor degreasing.

More components

Extending the fundamental idea that separation boundaries correspond to maximum line integrals to mixtures of four or more components is reasonably straightforward. For example, for a quaternary mixture, the line integral in Eq. 2 becomes a surface area integral, $B(x_0, \varepsilon)$ becomes a sphere instead of a circle, and thus there are two independent angles of rotation, say θ_1 and θ_2, that map feasible initial conditions $x(0)$ to points on the ε-sphere. Here the surface area is written in the form

$$A = \int\int [x'(\alpha_1, \alpha_2)] d\alpha_1 d\alpha_2 \tag{12}$$

where $x(\alpha_1, \alpha_2)$ is parameterized over the domain of interest. Therefore the area $A(\theta_1, \theta_2)$ becomes the objective function of interest for determining a separation boundary in a four-component mixture and separation boundaries—made up of a family of trajectories—are actually local maxima in the surface area defined in Eq. 12. Think of this as trying to determine θ_1 and θ_2 so as to maximize the area of the flexible balloon that lies within a given separation region. For five-component mixtures the surface area becomes a volume integral and $B(x_0, \varepsilon)$ is then an ε-hypersphere with three independent angles of rotations, for which each separation boundary is a local maximum in volume. Therefore for any c-component mixture the objective function will involve $c - 2$ integrations of $c - 2$ independent families of parameterized curves, $B(x_0, \varepsilon)$ will be an ε-hypersphere in R^{c-2}, and there will be $c - 2$ independent angles of rotation that uniquely map feasible initial conditions onto some part of $B(x_0, \varepsilon)$. We refer the reader to any text on differential geometry (see, for example, Thorpe[40]) for the details of surface area and volume integrals in terms of vector fields.

Reactive systems

Barbosa and Doherty[15-17] successfully extended the idea of simple distillation and residue curves to reacting mixtures and the underlying concepts have been very useful in the process synthesis and design of reactive separations. For equilibrium reactions, the composition variables that appear in Eq. 1 (or equivalently Eq. 3) are replaced by transformed variables of the form

$$y_i \rightarrow [(y_i/\nu_i) - (y_k/\nu_k)]/[\nu_k - \nu_T y_k] \tag{13}$$

$$x_i \rightarrow [(x_i/\nu_i) - (x_k/\nu_k)]/[\nu_k - \nu_T x_k] \tag{14}$$

where $\nu_T = \Sigma\, \nu_j$ is the sum of the stoichiometric coefficients ν_j, and the subscript k in Eqs. 13 and 14 denotes a reference species. We refer the reader to the work of Barbosa and Doherty for details. The important point here is that the equations describing simple distillation of reacting mixtures retain the form and underlying dynamical behavior of Eq. 1. That is, in reacting systems, reactive azeotropes play the role of azeotropes for nonreacting mixtures. Moreover, the properties of the fixed points of Eq. 1 remain the same for reacting mixtures. These reactive azeotropes, together with the pure component vertices, are still either unstable, saddle, or stable nodes of Eq. 1 for the transformed variables in Eqs. 13 and 14. Therefore, the proposed geometric approach as described in previous sections can be applied directly to rigorously determine separation boundaries for reactive mixtures. We conjecture that separation boundaries for reactive mixtures are still characterized by local maxima in line integrals, surface area, volume, and so forth in this transformed composition space. Moreover, we believe that similar results hold for kinetically limited reactions.

Nonequilibrium processes

Recently, Taylor et al.[41] combined mass transfer models with the theory of simple distillation and extended the concept of residue curve maps to nonequilibrium stagewise and packed distillation columns. One of the important attributes of the proposed geometric approach to separation boundaries is that it applies equally well to equilibrium and nonequilibrium processes. The only mathematical concerns in this regard have to do with the relationship between the composition variables y and x in Eq. 1. Nothing that has been developed in this presentation relies on any specific relationship between y and x. Therefore y and x can be related through equilibrium thermodynamics or through a nonequilibrium approach. Thus we believe (and of course this is a conjecture at this point) that because the geometric approach to separation boundaries that has been proposed is independent of the y–x relationship, that separation boundaries for ternary nonequilibrium processes also correspond to local maxima in the line integral. We further believe that extensions of the approach to larger numbers of components, heterogeneous behavior, reactive mixtures, and so on carry over to nonequilibrium models in very straightforward ways.

Other separations and processes

The form of Eq. 1 is actually quite appropriate for processes based on condensation cooling such as crystallization and vapor degreasing. Fractional crystallization is important in the pharmaceutical and drug industries, whereas vapor degreasing is a cleaning process that is widely used in a large number of industries (such as in the cleaning of metal parts, airplane parts, electronics, medical equipment, and so on). The application of line, surface area, and volume integrals to determining separation boundaries in processes such as crystallization is also possible. In crystallization, the differential equations (such as Eq. 1) remain the same, whereas the vector y represents the solid phase (or crystal) and x denotes the liquid phase (see

Slaughter and Doherty[18]). Both homogeneous and heterogeneous solid behavior is possible and minimum, maximum, and intermediate melting eutectic points (that is, points of melting or fusion that occur at constant composition) can exist (see, for example, Figures 5.22 and 5.23 in Walas[42]). These eutectic points take on the role that azeotropic points have in distillation. That is, eutectics can be either stable, unstable, or saddle nodes associated with the governing differential equations and, along with the pure component vertices, help define the separation boundaries in melt crystallization. Another interesting application in which separation boundaries are important is the precipitation and separation of solid wax.

Vapor degreasing, on the other hand, is a cleaning process that can be viewed as the exact opposite of simple distillation. Here, hot solvent vapors enter a chamber and condense on a cool, dirty part to effect cleaning. Solvents for cleaning metal parts, medical equipment, ink rollers, and other equipment are heavily regulated by the EPA and other environmental groups and recent applications have concentrated on the use of two or more cosolvents to clean multiple contaminants. These cosolvents often form multiple azeotropes with volatile contaminants (see Lucia and Finger[43]) and, as a result, there are separation boundaries that occur that can determine the degree of cleaning that can be achieved in vapor degreasing. Certainly, the geometric approach proposed in this work is directly applicable and thus we are also interested in its application to the design of vapor degreasers and any related solvent-recovery task needed to reuse valuable solvent.

The proposed geometric approach to separation boundaries has opened up a wide variety of interesting and challenging theoretical and algorithmic questions associated with the synthesis and design of separation processes as outlined in the coda. We are currently vigorously pursuing these and other related issues.

Acknowledgments

A. Lucia thanks the National Science Foundation for financial support under Grant No. CTS-0113091. The authors also thank Leah Octavio for preparing all of the figures.

Literature Cited

1. Doherty MF, Perkins JD. On the dynamics of distillation processes—I: The simple distillation of multicomponent, nonreacting homogeneous mixtures. *Chem Eng Sci.* 1978;33:281-301.
2. Pöllmann P, Blass E. Best products of homogeneous azeotropic distillations. *Gas Sep Purif.* 1994;8:194-228.
3. Fien G-JAF, Liu YA. Heuristic synthesis and shortcut design of separation processes using residue curve maps: A review. *Ind Eng Chem Res.* 1994;33:2505-2522.
4. Widagdo S, Seider WD. Azeotropic distillation. *AIChE J.* 1996;42:96-128.
5. Kiva VN, Hilmen EK, Skogestad S. Azeotropic phase equilibrium diagrams: A survey. *Chem Eng Sci.* 2003;58:1903-1953.
6. Petlyuk FB. *Distillation Theory and Its Application to Optimal Design of Separation Units*. Cambridge, UK: Cambridge Univ. Press; 2004.
7. Ostwald W. Dampfdrucke ternarer gemische. Abahndlungen der Mathematisch-Physischen der Konig Sachsischen. *Gesellschaft Wissenschaften.* 1900;25:413.
8. Ostwald W. *Lehrbuk der allgemeinen Chemie*. Leipzig, Germany: Engelmann; 1902.
9. Schreinemakers FAH. Dampfdrucke ternarer gemische. I: Theoretischer teil. *Z Phys Chem.* 1901;36:257-289.
10. Schreinemakers FAH. Dampfdrucke ternarer gemische. II: Theoretischer teil. *Z Phys Chem.* 1901;36:413-449.
11. Schreinemakers FAH. Dampfdrucke ternarer gemische. III: Theoretischer teil. *Z Phys Chem.* 1901;36:710-740.
12. Doherty MF, Perkins JD. On the dynamics of distillation processes—III: The topological structure of ternary residue curve maps. *Chem Eng Sci.* 1979;34:1401-1414.
13. Pham HN, Doherty MF. Design and synthesis of heterogeneous azeotropic distillations. *Chem Eng Sci.* 1990;45:1823-1836.
14. Pham HN, Doherty MF. Design and synthesis of heterogeneous azeotropic distillations. *Chem Eng Sci.* 1990;45:1837-1844.
15. Barbosa D, Doherty MF. The influence of chemical reactions on vapor–liquid phase diagrams. *Chem Eng Sci.* 1988;43:529-540.
16. Barbosa D, Doherty MF. The simple distillation of homogeneous reactive mixture. *Chem Eng Sci.* 1988;43:541-550.
17. Barbosa D, Doherty MF. Design and minimum reflux calculations for single-feed multicomponent reactive distillation columns. *Chem Eng Sci.* 1988;43:1523-1537.
18. Slaughter DW, Doherty MF. Calculation of solid–liquid equilibrium and crystallization paths for melt crystallization processes. *Chem Eng Sci.* 1995;50:1679-1694.
19. Doherty MF, Malone MF. *Conceptual Design of Distillation System*. New York, NY: McGraw-Hill; 2001.
20. Van Dongen DB, Doherty MF. On the dynamics of distillation processes vs. the topology of the boiling temperature surface and its relation to azeotropic distillation. *Chem Eng Sci.* 1984;39:883-892.
21. Foucher ER, Doherty MF, Malone MF. Automatic screening of entrainers for homogeneous azeotropic distillation. *Ind Eng Chem Res.* 1991;29:760-772.
22. Peterson EJ, Partin LR. Temperature sequences for categorizing all ternary distillation boundary maps. *Ind Eng Chem Res.* 1997;36:1799-1811.
23. Rooks RE, Julka V, Doherty MF, Malone MF. Structure of distillation regions for multicomponent azeotropic mixtures. *AIChE J.* 1988;44:1382-1391.
24. Pöpken T, Gmehling J. Simple method for determining the location of distillation region boundaries in quaternary systems. *Ind Eng Chem Res.* 2004;43:777-783.
25. Lucia A, Yang F. Multivariable terrain methods. *AIChE J.* 2003;49:2553-2563.
26. Levy AV, Montalvo A. The tunneling method for the global minimization of functions. *SIAM J Sci Stat Comp.* 1985;6:15-29.
27. Maranas CD, Floudas CA. Finding all solutions to nonlinearly constrained systems of equations. *J Global Optim.* 1995;7:153-182.
28. Schnepper CA, Stadtherr MA. Robust process simulation using interval methods. *Comput Chem Eng.* 1996;20:187-199.
29. Lucia A, Yang F. Global terrain methods. *Comput Chem Eng.* 2002;26:529-546.
30. Lucia A, DiMaggio PA, Depa K. A geometric terrain methodology for global optimization. *J Global Optim.* 2004;29:297-314.
31. Metropolis N, Rosenbluth A, Rosenbluth M, Teller A, Teller E. Equation of state calculations by fast computing machines. *J Chem Phys.* 1953;21:1087-1092.
32. Kirkpatrick S, Gelatt CD, Vecchi MP. Optimization by simulated annealing. *Science.* 1989;220:671-680.
33. Aluffi-Pentini F, Parisi V, Zirilli F. Global optimization and stochastic differential equations. *J Opt Theory Appl.* 1985;47:1-17.
34. Lucia A, Bellows ML, Octavio LM. Global optimization of ordinary differential equations models. In: Puigjaner L, Espuna A, eds. *European Symposium on Computer Aided Process Engineering*. Amsterdam: Elsevier BV; 2005:115-120.
35. Venkataraman S, Lucia A. Solving distillation problems by Newton-like methods. *Comput Chem Eng.* 1988;12:55-69.
36. Lucia A, DiMaggio PA. Non-quadratic methodologies for process optimization. In: Floudas CA, Agarwal R, eds. *Foundations of Computer-Aided Process Design*. Austin, TX: CACHE Corp.; 2004:561-564.
37. Prausnitz JM, Anderson TF, Grens EA, Eckert CA, Hsieh R, O'Connell JP. *Computer Calculations for Multicomponent Vapor–Liquid and Liquid–Liquid Equilibria*. Engelwood Cliffs, NJ: Prentice-Hall; 1980.
38. Renon H, Prausnitz JM. Estimation of parameters for the NRTL equation for excess Gibbs energies of strongly non-ideal liquid mixtures. *Ind Eng Chem Res.* 1969;8:413-419.
39. Gmehling J, Onken U. *Vapor–Liquid Equilibrium Data Collection*. Frankfurt, Germany: DECHEMA/Prentice-Hall; 1977.

Table A1. Pure Component Constants for Extended Antoine Equation

Component	c_1	c_2	c_3	c_4	c_5	c_6
Chloroform	0.065975	−29.011	0	-3.0001×10^{-5}	54.74	0.27483
Methanol	0.137610	−57.722	0	-5.9496×10^{-5}	80.94	0.23181
Ethanol	−0.062301	20.486	0	2.0664×10^{-5}	63.80	0.25202
Acetone	−0.14358	46.384	0	6.3961×10^{-5}	47.60	0.24702
Benzene	0.019082	−14.212	0	-6.7182×10^{-6}	48.98	0.26963
Water	0.0035888	−6.6689	0	-8.5084×10^{-7}	221.20	0.2380
Methanol	23.40247	3593.39	35.225	0	0	0
Acetone	21.62497	2975.95	34.523	0	0	0
Methylacetate	21.61517	2917.70	41.372	0	0	0

Table A2. Binary Interaction Parameters for the UNIQUAC Equation

Component i	Component j	a_{ij} (K)	a_{ji} (K)
Chloroform	Methanol	926.31	−143.50
Chloroform	Acetone	93.96	−171.71
Chloroform	Benzene	4.98	−50.53
Methanol	Acetone	−96.90	359.10
Methanol	Benzene	−86.89	1284.21
Ethanol	Benzene	−128.88	997.41
Ethanol	Water	−64.56	380.68
Acetone	Benzene	−108.79	174.00
Benzene	Water	2057.42	115.13

40. Thorpe JA. *Elementary Topics in Differential Geometry*. New York, NY: Springer-Verlag; 1979.
41. Taylor R, Baur R, Krishna R. Influence of mass transfer in distillation: Residue curves and total reflux. *AIChE J.* 2004;50:3134-3148.
42. Walas SM. *Phase Equilibria in Chemical Engineering*. Stoneham, MA: Butterworth; 1985.
43. Lucia A, Finger EJ. Co-solvent selection and recovery. *Adv Environ Res.* 2003;8:197-211.

Appendix

The relevant physical property data for the examples studied herein are the binary interaction parameters for the UNIQUAC and NRTL activity coefficient models and the constants required to compute standard state fugacities for each component in the liquid phase.

The standard state liquid-phase component fugacities can be expressed using an Antoine or extended Antoine equation of the form

$$\ln f_i^0 = c_{i,1} + c_{i,2}/(T + c_{i,3}) + c_{i,4}T + c_{i,5}\ln(T) + c_{i,6}T^2 \tag{A1}$$

Table A3. Binary Interaction Parameters for the NRTL Equation*

Component i	Component j	b_{ij} (cal/gmol)	b_{ji} (cal/gmol)	α_{ij}
Methanol	Acetone	226.558	184.2662	0.3009
Methanol	Methylacetate	346.536	381.4559	0.2965
Acetone	Methylacetate	88.795	75.0543	0.3021

*The data are reproduced from Gmehling and Onken[39] in their original form. The appropriate conversion to SI units is 1 cal/gmol = 4184.275 J/kg mol.

where f_i^0 has units of 10^5 Pa. Table A1 gives the numerical values of the pure component constants in Eq. A1. The first group of constants were used in Examples 1, 2, and 4, whereas the second group of constants were used for Example 3.

The temperature-dependent interaction terms τ_{ij} for the UNIQUAC equation of Prausnitz et al.[37] are expressed in the form

$$\tau_{ij} = \exp(-a_{ij}/T) \tag{A2}$$

where a_{ij} represent binary interaction parameters. Table A2 gives the binary interaction parameters for the UNIQUAC equation for the chemical species used herein.

Temperature-dependent interaction terms, τ_{ij} and G_{ij}, for the NRTL equation of Renon and Prausnitz[38] are expressed in the form

$$\tau_{ij} = \exp(a_{ij} + b_{ij}/RT) \qquad \text{and} \qquad G_{ij} = \exp(\alpha_{ij}\tau_{ij}) \tag{A3}$$

where a_{ij} and b_{ij} are binary interaction parameters. In this work, all a_{ij} values were set to zero. Values for the b_{ij} and α_{ij} parameters are given in Table A3.

Manuscript received Jan. 5, 2005, and revision received Jun. 22, 2005.